Supporting Information

Photosalient effect and reversible photochromic photoluminescence driven by cascade [2+2] cycloaddition reaction and water adsorption in 0D hybrid metal halide

Chudong Chen[a,b], Ziquan Li[b], Yonghong Xiao[b], Chenghao Ye[c], Jianwu Wei[a], Ruosheng Zeng[d], Qi Pang[a] and Binbin Luo[a,*]

[a] *School of Chemistry and Chemical Engineering and Key Laboratory of Electrochemical Energy Materials, Guangxi University, Nanning 530004, P. R. China*

[b] *College of Chemistry and Chemical Engineering, Shantou University, Shantou, 515063, P. R. China*

[c] *School of Power and Mechanical Engineering, Wuhan University, Wuhan 430072, P. R. China*

[d] *School of Physical Science and Technology/State Key Laboratory of Featured Metal Materials and Life-cycle Safety for Composite Structures, Guangxi University, Nanning 530004, P. R. China*

Corresponding Author: bbluo@gxu.edu.cn

Table of Contents

EXPERIMENTAL SECTION

Materials and methods

4-Styrylpyridine (**L**, 98%, Adamas), indium chloride (99.99%, Aladdin), hydrochloride acid (37%, Guanghua Sci-Tech), ethyl acetate (EA, 99.7%, Guanghua Sci-Tech), ethanol (99.7%, Guanghua Sci-Tech), polymethyl methacrylate (PMMA, 98%, Wangda Plastic), dimethyl sulfoxide-d_6 (DMSO-d_6, 99.8%, J&K), paraffin oil (100%, Hampton Research). All chemicals were used without further purification.

Synthesis of LH·Cl and LH·Cl-450

0.0181 g of **L** were dissolved in 500 μL concentrated HCl at 120 ℃ in the sealed pressure bottle, the solution was cooled to room temperature without perturbation, and **LH**·Cl was obtained overnight with a yield of 77.7%. ^{1}H NMR (400 MHz, DMSO-d_6): δ 8.85 (d, J = 6.1 Hz, 2H), 8.22 (d, J = 6.2 Hz, 2H), 8.02 (d, J = 16.4 Hz, 1H), 7.82 – 7.71 (m, 2H), 7.56 (d, J = 16.4 Hz, 1H), 7.53 – 7.38 (m, 3H). **LH**·Cl-450 was obtained through irradiating **LH**·Cl with 450 nm light for 0.5 h. ^{1}H NMR (400 MHz, DMSO-d_6): δ 8.74 (d, J = 6.3 Hz, 4H), 7.94 (d, J = 6.2 Hz, 4H), 7.28 (d, J = 7.2 Hz, 4H), 7.21 (t, J = 7.5 Hz, 4H), 7.11 (t, J = 7.3 Hz, 2H), 5.08 – 4.90 (m, 4H).

Synthesis of $(LH)_2InCl_5$ single crystals

$(LH)_2$ $InCl_5$ (**1**) single crystals were synthesized by loading 0.10 mmol **L**, 0.05 mmol indium chloride into a 15.0 mL pressure bottle containing 1.00 mL concentrated HCl. After all reactants were dissolved at 120 ℃ (the temperature of hot plate) in the sealed pressure bottle, the solution was cooled to room temperature without perturbation, and the yellow block crystals of **1** with a yield of 38.1% were obtained overnight. ^{1}H NMR (600 MHz, DMSO-d_6, ppm): δ 8.84 (d, J = 6.8 Hz, 2H), 8.20 (d, J = 6.1 Hz, 2H), 8.00 (d, J = 16.4 Hz, 1H), 7.76 (d, J = 8.8 Hz, 2H), 7.55 (dd, J = 16.4, 1.8 Hz, 1H), 7.48 (ddd, J = 7.8, 6.4, 1.6 Hz, 2H), 7.44 (td, J = 7.1, 1.7 Hz, 1H).

Synthesis of $(L_2H_2)_2[In(H_2O)Cl_5][InCl_5]$single crystals

1 single crystals, wrapped in PN oil, were placed on microscope slides and exposed to 450 nm light at 223 K for about 30 minutes, then **$(L_2H_2)_2$**$[In(H_2O)Cl_5][InCl_5]$ (**1i**) single crystals were obtained. The distance between the light source and the sample was about 10 cm.

Synthesis of $(L_2H_2)[In(H_2O)Cl_5]$ single crystals

$(\mathbf{L_2H_2})[In(H_2O)Cl_5]$ (**1a**) single crystals were obtained through irradiating **1** single crystals on microscope slides with 450 nm light at 223 K for ~30 minutes. The distance between the light source and the samples was about 10 cm. ^{1}H NMR (600 MHz, DMSO-d_6, ppm): δ 8.71 (d, J = 5.1 Hz, 4H), 7.91 (d, J = 6.1 Hz, 4H), 7.28 (d, J = 8.2 Hz, 4H), 7.21 (td, J = 7.7, 1.5 Hz, 4H), 7.11 (td, J = 7.3, 1.4 Hz, 2H), 4.98 (ddd, J = 60.6, 10.8, 7.8 Hz, 4H).

Synthesis of 1-PMMA film

First, 1.0 g of PMMA was dissolved in EA with a volume of 30.0 mL. Subsequently, 0.20 g of finely ground **1** powder was added, followed by ultrasonic treatment for 15 minutes. Then, 7.0 mL of the thus-prepared mixed solution was transferred into a polytetrafluoroethylene culture dish. After being left to stand for 4 hours at room temperature, the **1**-PMMA film was obtained via the evaporation of EA solvent.

Characterization

Single crystal X-ray diffraction (SC-XRD). SC-XRD tests were conducted on Rigaku XtaLab Pro MM007HF DWX diffractometer at 293 K for **1** and 200 K for **1i** and **1a** using Cu Kα radiation (λ = 1.5418 Å). The structures were solved by intrinsic phasing method using SHELXT[1] program implanted in Olex2.[2] Refinement with full matrix least squares techniques on F^2 was performed by using SHELXL.[3] Non-hydrogen atoms were anisotropically refined and all hydrogen atoms were generated based on riding mode.

Powder XRD. PXRD patterns were recorded on MiniFlex 600 (Rigaku) to examine the crystalline phase.

UV-vis diffuse reflectance spectroscopy. UV-vis spectra were measured on Lambda 950 UV-vis Spectrometer (PerkinElmer).

Photoluminescence (PL) spectrum. PL spectra were collected on PTI QM-TM (Photon Technology International).

^{1}H nuclear magnetic resonance (^{1}H-NMR) spectra. ^{1}H-NMR spectra were recorded with a Bruker Advance 600 MHz spectrometer using DMSO-d_6 as solvents.

Fourier transform infrared (FTIR) spectra. FTIR spectra were measured on Thermo Fisher

Scientific (Nicolet AVATAR 360).

Thermogravimetry analysis (TGA). TGA curve was recorded on TA TGA550 with a heating rate of 5 °C/min.

Scanning electron microscope (SEM) and Energy dispersive spectroscopy (EDS) mapping. SEM images and EDS mapping (JSM-7500F, JEOL) were carried out to obtain the morphology and elemental distribution.

Transmission Electron Microscopy (TEM) and EDS mapping. TEM images and EDS mapping (JEM-F200, JEOL) were carried out to obtain the morphology and elemental distribution.

Hirshfeld surface analysis. The Hirshfeld surface was calculated by using the Crystal Explorer software based on the crystal structures.[4]

Free volume calculation. Free volume was calculated by using the Mercury software based on the crystal structures, the probe radius and approx. grid spacing are set as 1.0 Å and 0.2 Å.

Computational Details. All density functional theory (DFT) calculations were performed using the ORCA 6.0.1 software package.[5-7] Geometries were optimized using the M06 functional[8] with a basis set of def2-SVP for all atoms. Vibrational frequencies were calculated for all the stationary points to confirm if each optimized structure is a local minimum on the respective potential energy surface or a transition state structure with only one imaginary frequency. The intrinsic reaction coordinate (IRC) calculations were carried out to confirm the located transition states connect the correct intermediates. The single-point energy was calculated at M06/def2-TZVP level.

We show constrained geometries optimization with C–C bond-forming distances fixed at 1.5 to 3.0 Å. These values are typical for the process of forming and breaking C–C distances in many pericyclic reactions. Constraint DFT optimization of the transition state based on the C–C bond-forming distances fixed at 2.0 Å gives the constrained transition states. The constrained transition states are not true first-order saddle points on the potential energy surface, but these transition states offer similar geometries for the cycloaddition transition states involving different dienes and allow us to solely focus on the coordinated effect toward the interaction energies and its components, without the complications of early and later or asynchronous transition states. The optimized reactants, products and transition state structures were plotted using CYLview.[9]

Table S1. Crystal data of **1**, **1i** and **1a**.

Sample	**1**	**1i**	**1a**
Empirical formula	$(C_{13}H_{12}N)_2InCl_5$	$(C_{26}H_{24}N_2)_2[In(H_2O)Cl_5][InCl_5]$	$(C_{13}H_{12}N)_2[In(H_2O)Cl_5]$
Formula weight	656.54	1331.10	674.56
Temperature/K	293(4)	200.00(10)	199.99(10)
Radiation	Cu Kα (λ = 1.54184 Å)	Cu Kα (λ = 1.54184 Å)	Cu Kα (λ = 1.54184 Å)
Crystal system	triclinic	triclinic	triclinic
Space group	$P\bar{1}$	$P\bar{1}$	$P\bar{1}$
a/Å	8.5802(5)	10.8121(3)	10.8192(4)
b/Å	9.2837(3)	15.0764(5)	11.7903(5)
c/Å	18.2358(3)	18.0060(4)	11.9138(5)
α/°	97.408(2)	90.349(2))	99.720(4)
β/°	98.221(3)	91.409(2)	92.935(3)
γ/°	105.005(4)	95.489(2)	98.493(3)
V/Å^3	1367.56(10)	2920.67(14)	1476.97(11)
Z	2	2	2
ρ_{calc} (g/cm^3)	1.594	1.514	1.517
completeness to θ_{max}	94.7%	95.0%	96.0%
GOF	1.083	1.059	1.048
R_{int}	0.0293	0.0786	0.0260
final *R* indexes [$I > 2\sigma(I)$][a]	R_1 = 0.0325, wR_2 = 0.0864	R_1 = 0.0641, wR_2 = 0.1612	R_1 = 0.0754, wR_2 = 0.2226
R indexes (all data)[a]	R_1 = 0.0367, wR_2 = 0.0884	R_1 = 0.1020, wR_2 = 0.1738	R_1 = 0.0844, wR_2 = 0.2337
largest diff. peak and hole, e Å^{-3}	0.54/-0.60	1.08/-1.42	1.76/-1.46

[a] $R_1 = \Sigma||F_o|-|F_c||/\Sigma|F_o|$; $wR_2 = \{[\Sigma w(F_o^2-F_c^2)^2]/\Sigma[w(F_o^2)^2]\}^{1/2}$; $w = 1/[\sigma^2(F_o^2)+(aP)^2+bP]$, where $P = [\max(F_o^2, 0) + 2Fc^2]/3$ for all data.

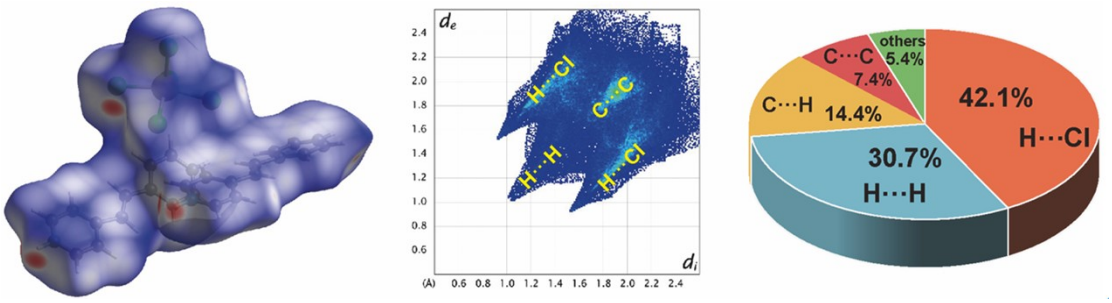

Figure S1. Hirshfeld surface view, 2D fingerprint plots, and the relative contributions of atomic contacts to the Hirshfeld surface of **1**.

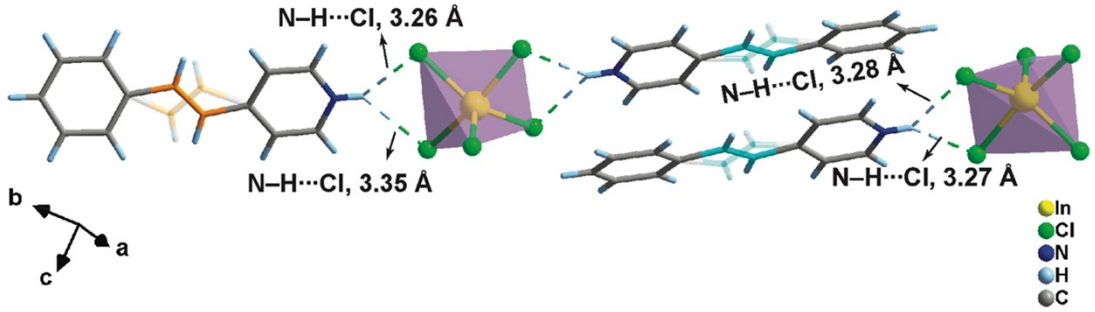

Figure S2. Hydrogen bonding interaction between $\mathbf{LH}^+$ dimer and $[InCl_5]^{2-}$ polyhedron in **1**.

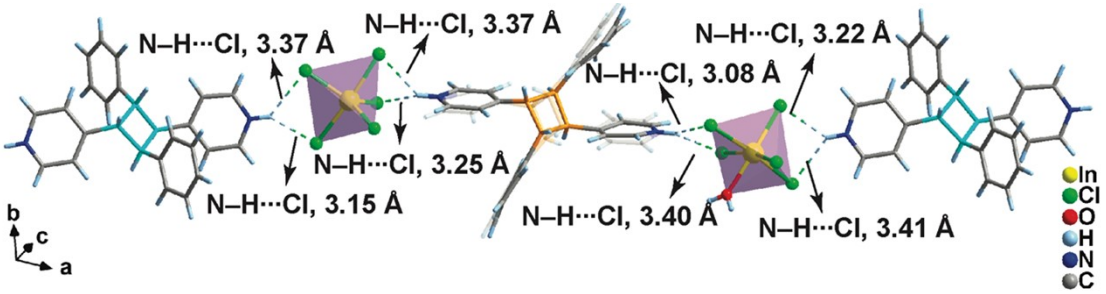

Figure S3. Hydrogen bonding interaction between $\mathbf{LH}^+$ photodimers and $[InCl_5{\cdot}H_2O]^{2-}$/$[InCl_5]^{2-}$ polyhedron in **1i**.

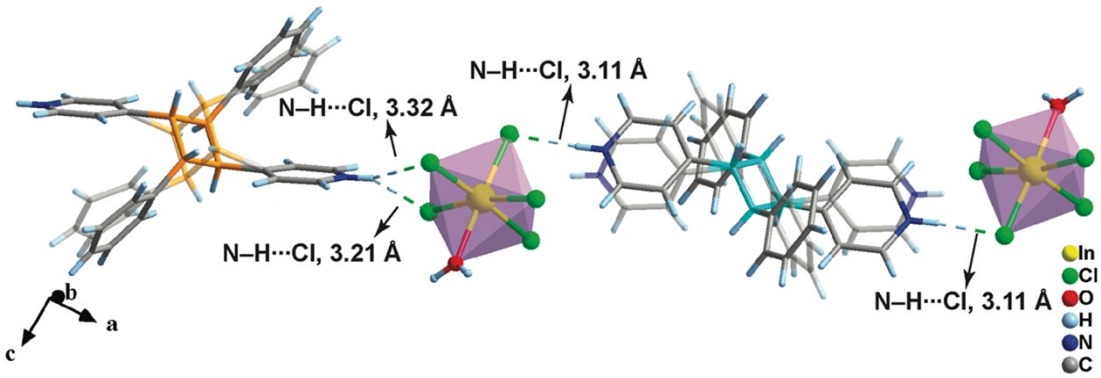

Figure S4. Hydrogen bonding interaction between $\mathbf{LH}^{+}$ photodimers and $[InCl_5 \cdot H_2O]^{2-}$ octahedron in **1a**.

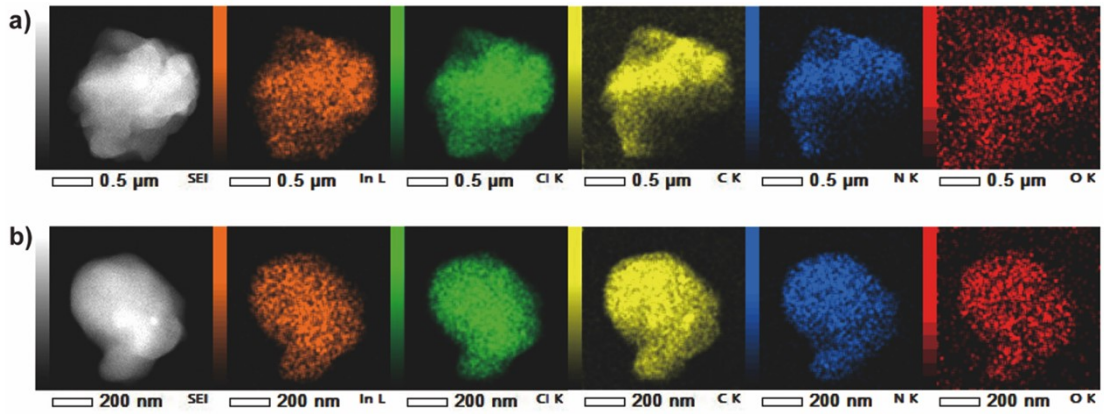

Figure S5. EDS mapping of In, Cl, C, N and O elements for (a) **1** and (b) **1a**.

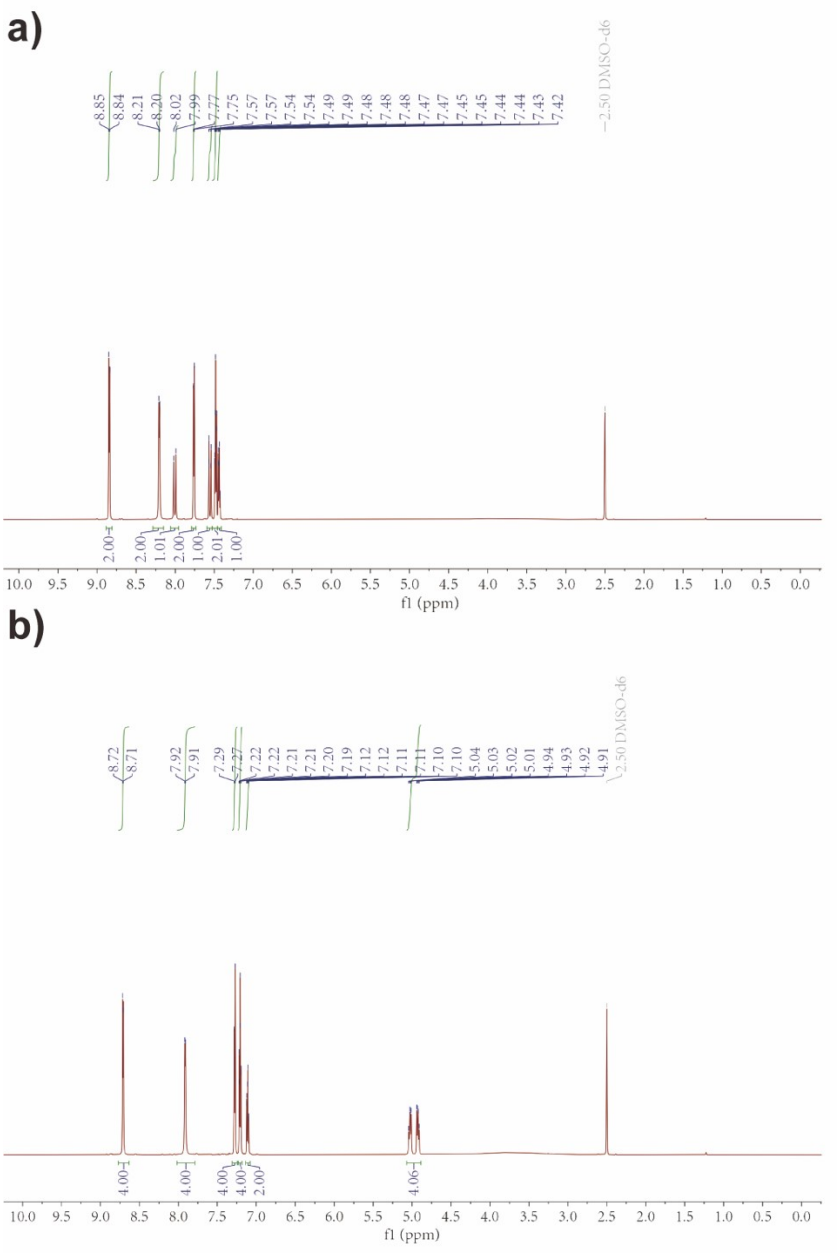

Figure S6. ^{1}H NMR spectrum of (a) **1** and (b) **1a** in DMSO-d_6.

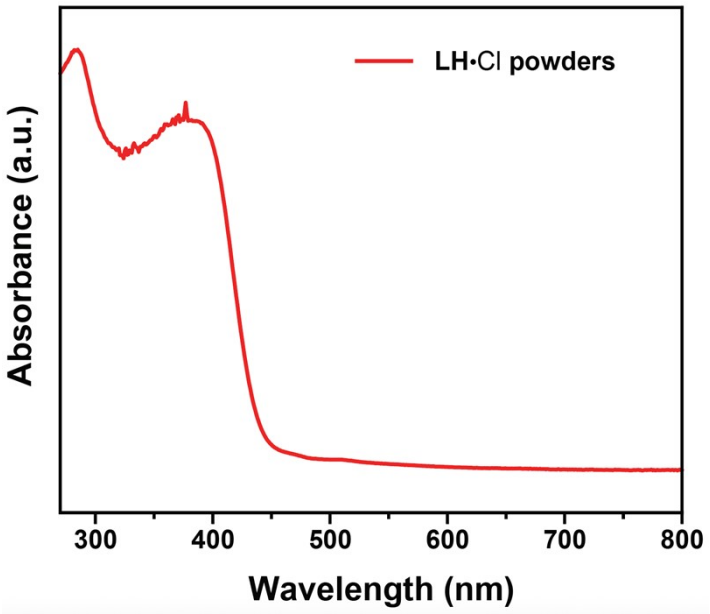

Figure S7. UV−vis diffuse reflectance spectrum of **LH**·Cl

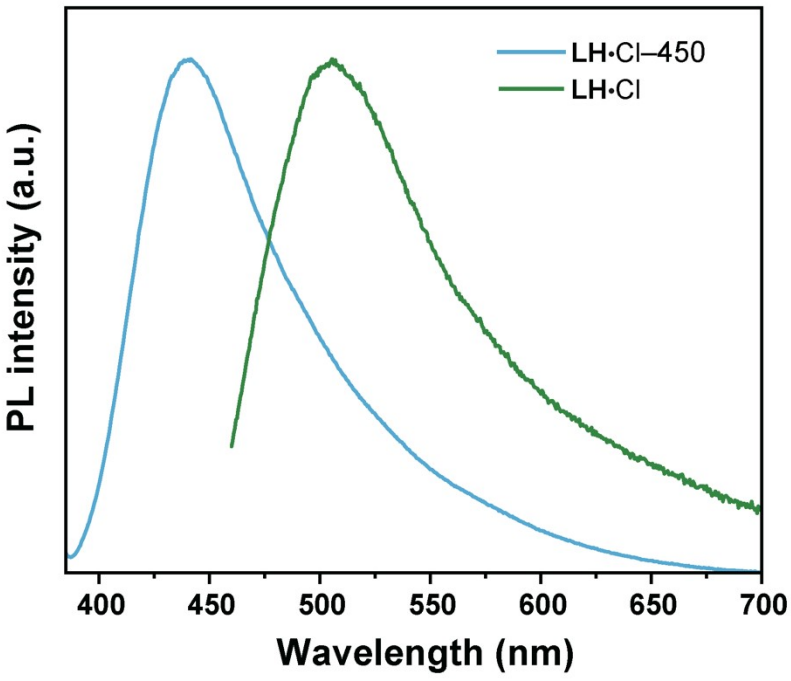

Figure S8. PL spectra of **LH**·Cl and **LH**·Cl-450 (**LH**·Cl powder irradiated at 450 nm for 10 minutes).

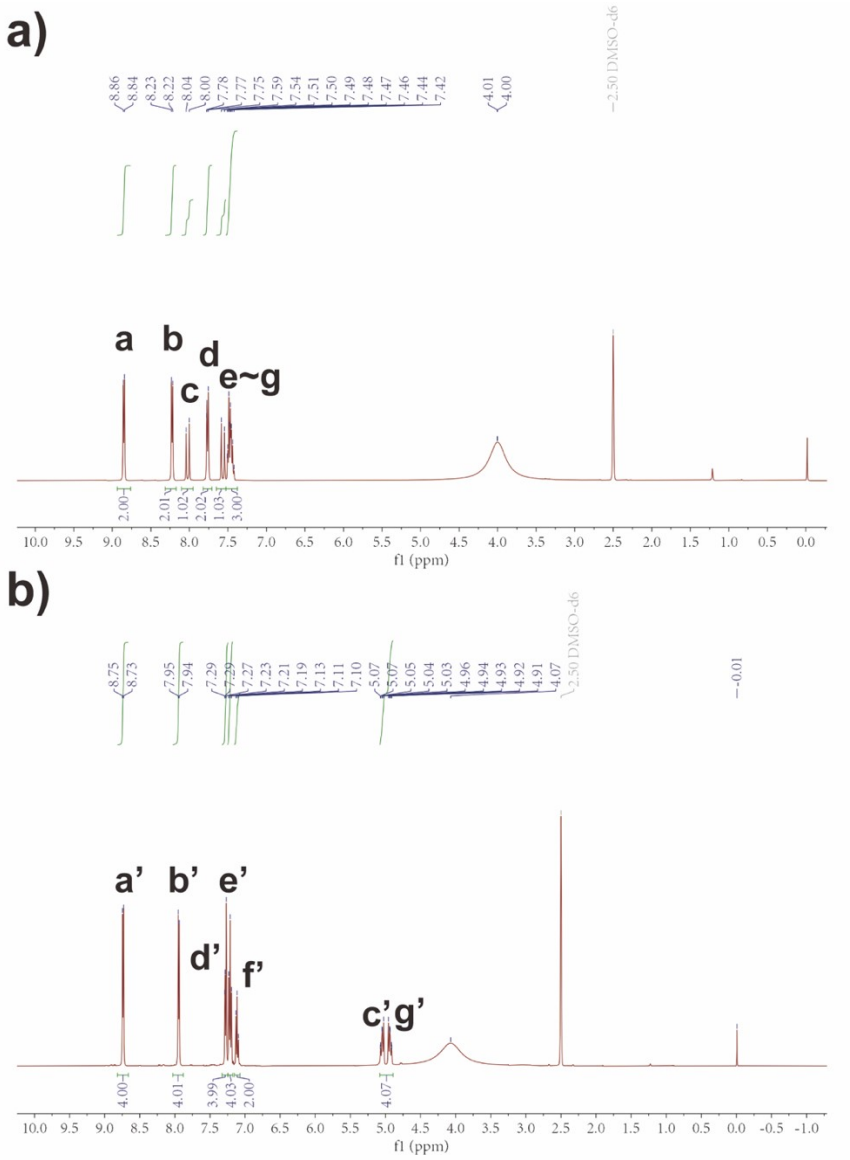

Figure S9. ^{1}H NMR spectrum of (a) **LH**·Cl and (b) **LH**·Cl-450 in DMSO-d_6.

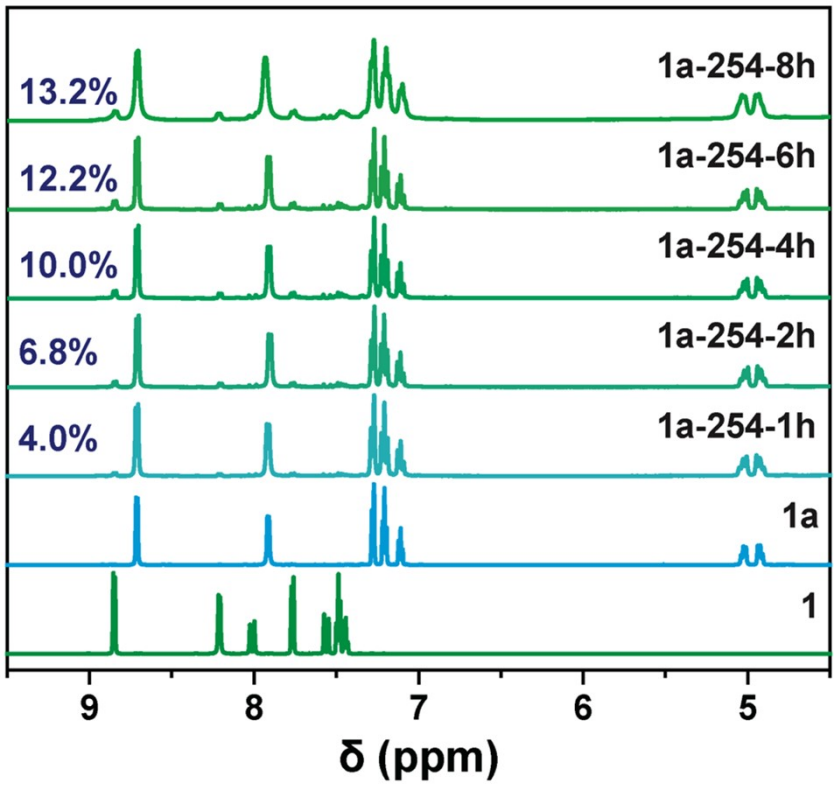

Figure S10. ^{1}H NMR spectra (solvent: DMSO-d_6) of **1a-254** with different irradiation time.

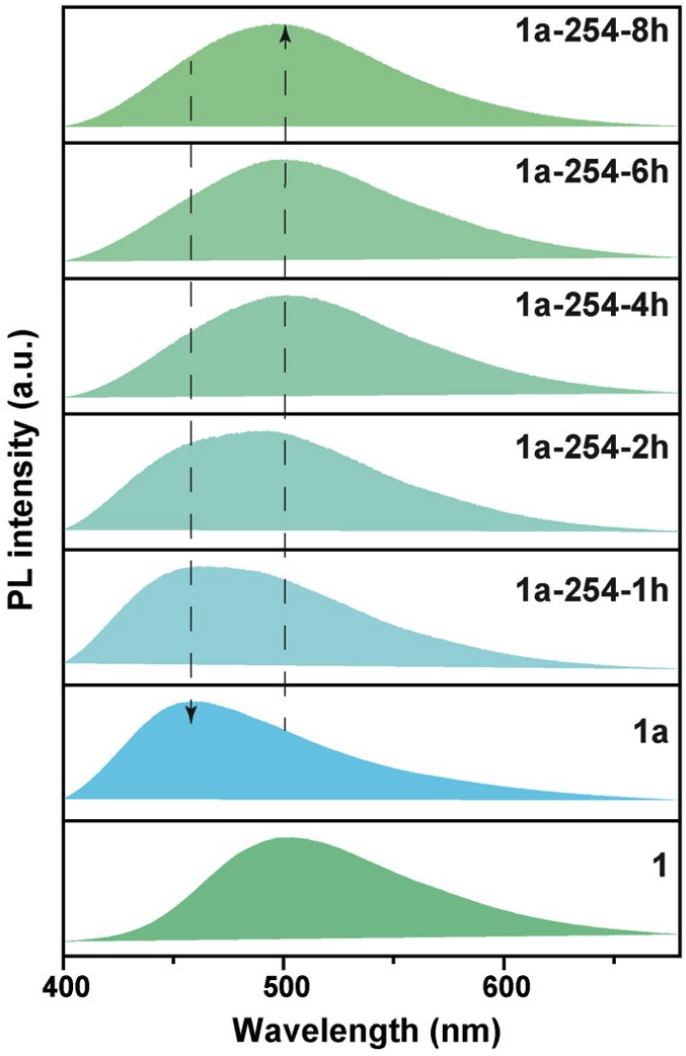

Figure S11. PL spectra of **1a-254** with different irradiation time.

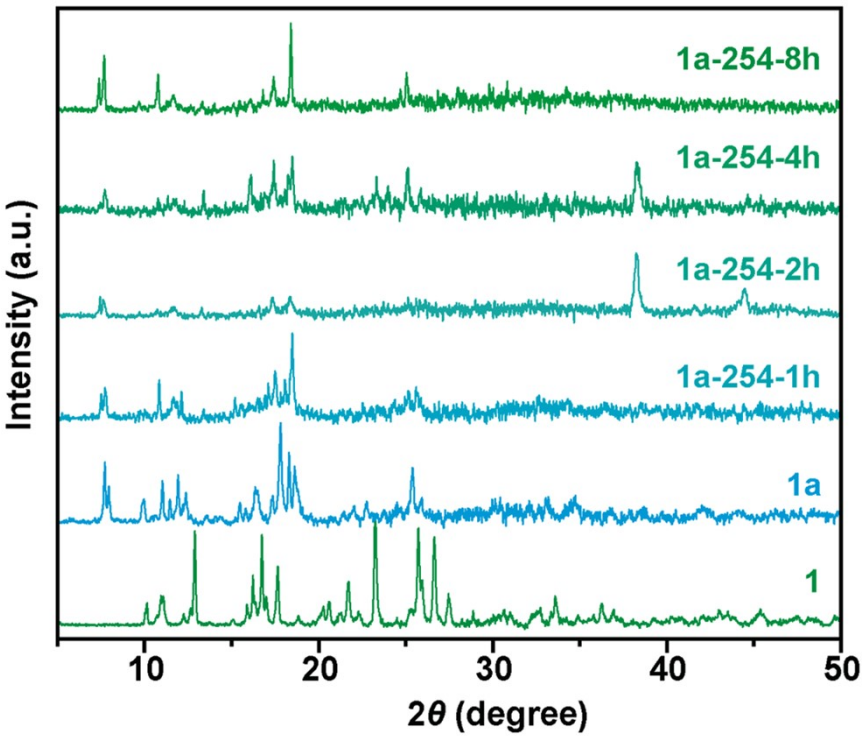

Figure S12. PXRD of **1a-254** with different irradiation time.

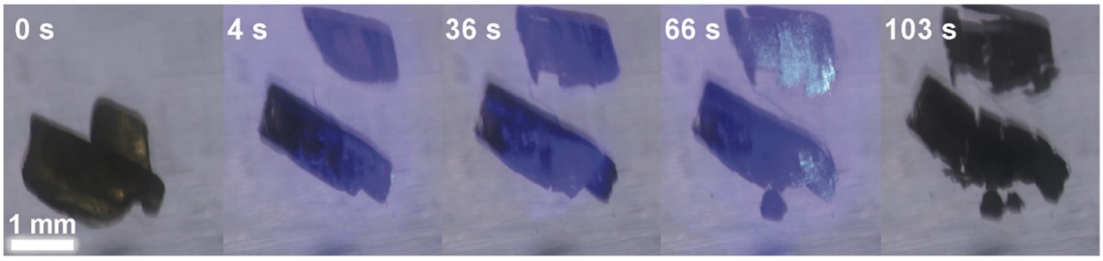

Figure S13. Images of **1** in Schlenk tube evacuated for 2 hours at 80 °C under the irradiation of 450 nm light (130 mW/cm^2).

Table S2. Photomechanical performance of some reported compounds.

Samples	Structural Type	Volume change	Light source	Photomechanical response	Reference
[Zn(bdc)(3-F-spy)]	CPs	–6.10%	365 nm	bending, splitting twisting	10
$[Cu_2(benzoate)_4(4spy)_2]$	CPs	+15.40%	365 nm	popping	11
$[Zn_2(cin)_4(4spy)_2]$	CPs	+11.93%	351 nm (150 W)	spurting	12
$[Zn(NCS)_2(2F\text{-}4spy)_2$	CPs	+17.60%	UV light	popping	13
$[Ag(2F\text{-}4spy)_2]BF_4$	CPs	+18.97%	UV light (28 W cm^{-2})	jumping, splitting	14
$(\mathbf{LH})_2InCl_5$	ICs	+8.0%	450 nm (130 mW cm^{-2})	explosion, bending breaking, jumping	This work

CPs: coordination polymers; MCs: molecular crystals; ICs: ionic crystals.

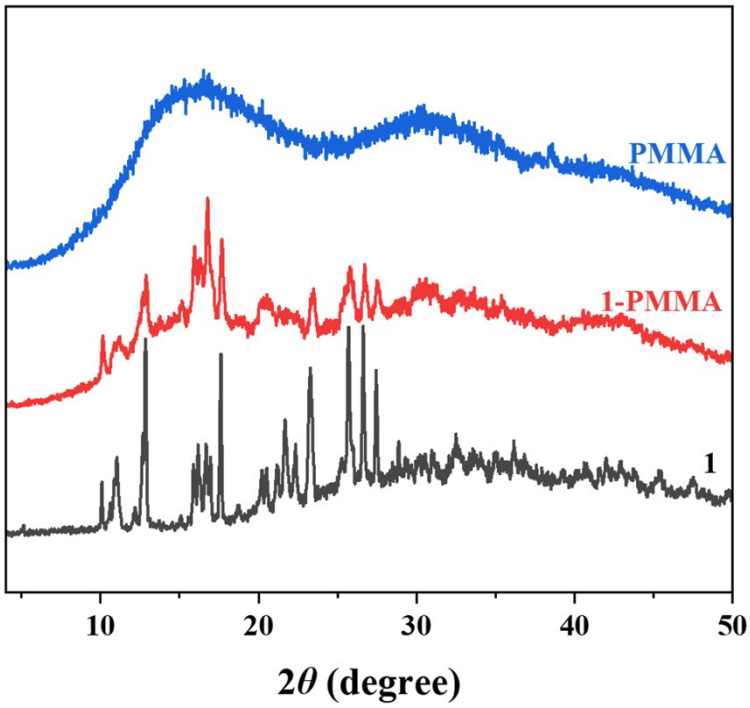

Figure S14. PXRD patterns of **1**, **1**-PMMA and PMMA.

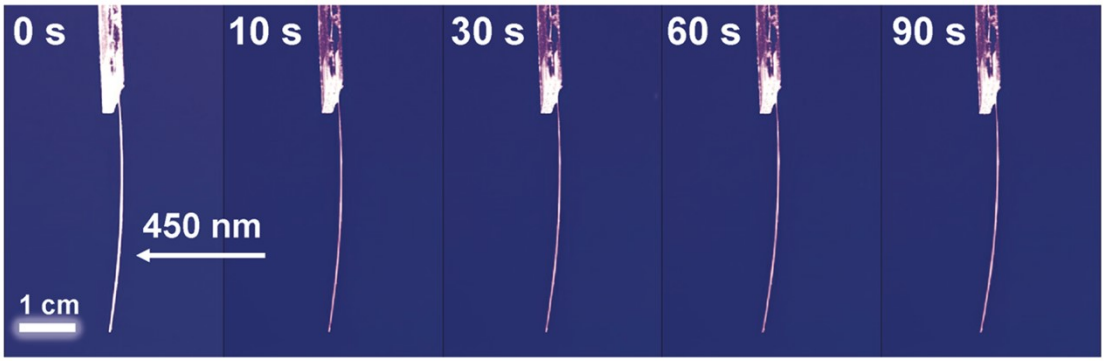

Figure S15. Images of PMMA film (0.5 cm × 4 cm) upon exposure to 450 nm light.

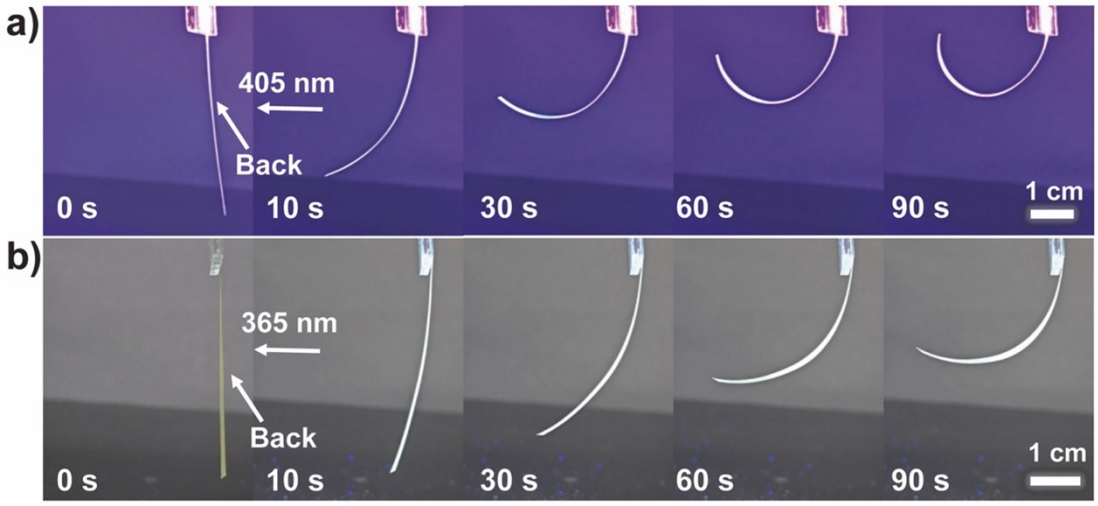

Figure S16. Images of **1**-PMMA film (0.5 cm × 4 cm) upon exposure to (a) 405 and (b) 365 nm light.

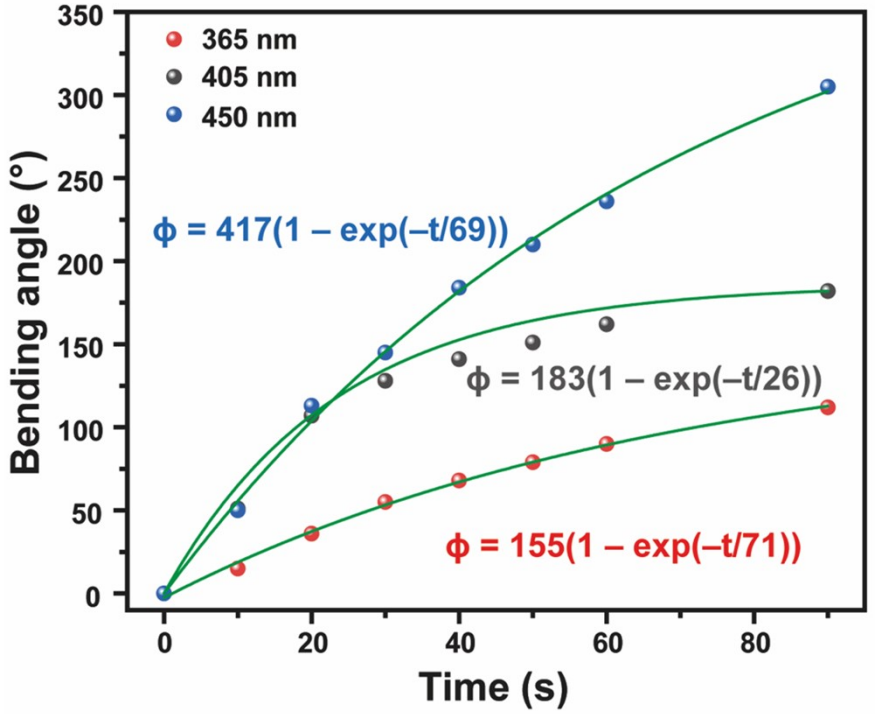

Figure S17. Fitting results of the bending angle as a function of exposure time for **1**-PMMA with different irradiation wavelengths.

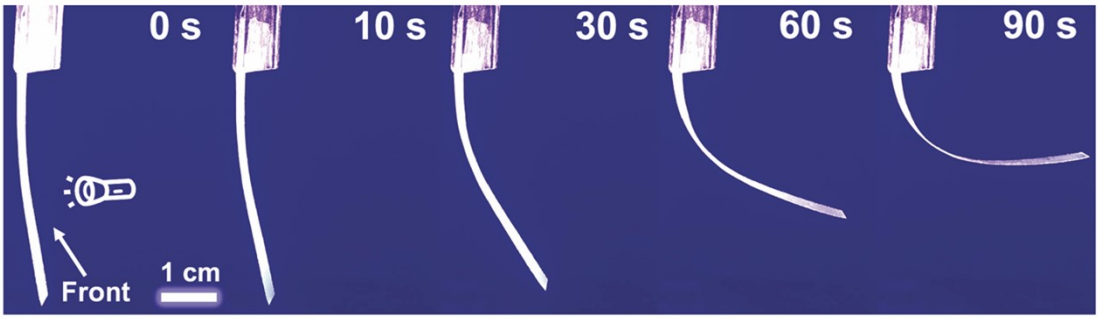

Figure S18. Images of the front side of **1**-PMMA (0.5 cm × 4 cm) upon exposure to 450 nm light.

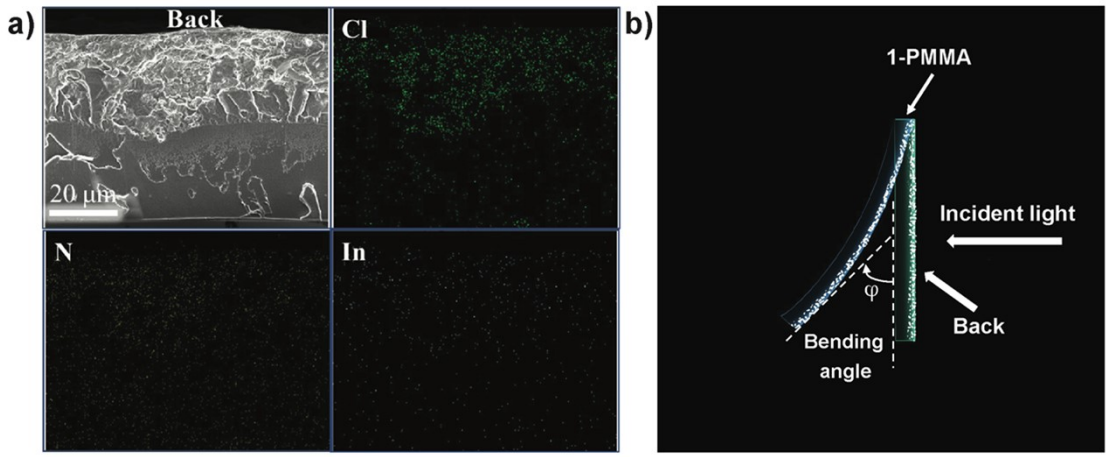

Figure S19. (a) SEM image and EDS mapping of In, Cl, N elements for the cross-section of **1**-PMMA. (b) Schematic illustration of the photoinduced bending for **1**-PMMA.

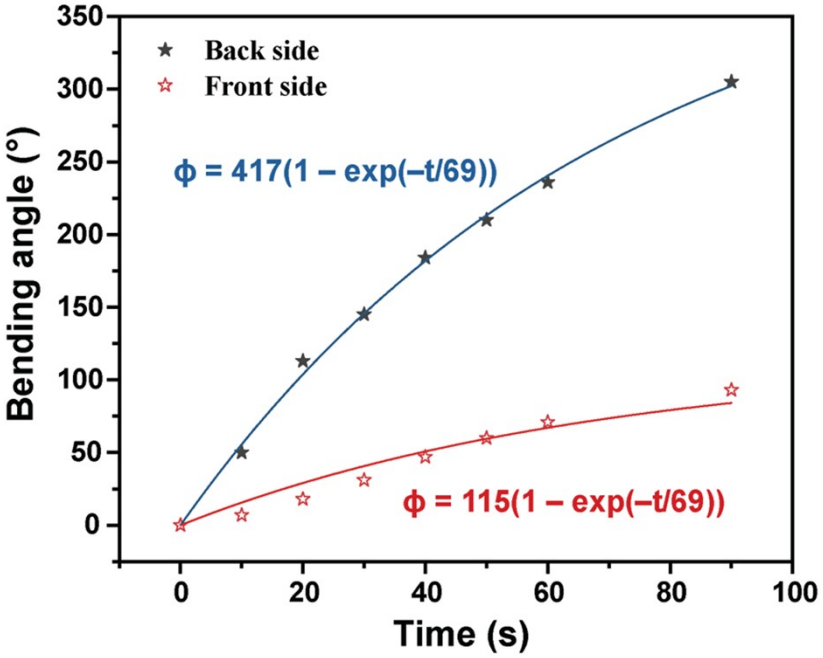

Figure S20. Fitting results of **1**-PMMA bending angles against exposure time.

Figure S21. Preparation of **1**-PMMA without (left) and with (right) concentration gradient.

REFERENCES

[1] Sheldrick, G. M., Shelxt-Integrated Space-Group and Crystal-Structure Determination. *Acta Cryst. A* **2015**, 71, 3-8.

[2] Dolomanov, O. V. B., L. J.; Gildea, R. J.; Howard, J. A. K.; Puschmann, H., Olex2: A Complete Structure Solution, Refinement and Analysis Program. *J. Appl. Crystallogr.* **2009**, 42, 339-341.

[3] Sheldrick, G. M., A Short History of Shelx. *Acta Cryst. A* **2008**, 64, 112-122.

[4] M. Turner, J. McKinnon, S. Wolff, D. Grimwood, P. Spackman, D. Jayatilaka, M. Spackman, *CrystalExplorer17*, The University of Western Australia, Australia, **2017**.

[5] Neese, F., An Improvement of the Resolution of the Identity Approximation for the Formation of the Coulomb Matrix. *J. Comput. Chem.* 2003, *24* (14), 1740-1747.

[6] Neese, F., Software update: The ORCA Program System—Version 5.0. *Wires: Comput. Mol. Sci.* 2022, *12* (5), e1606.

[7] Neese, F., The SHARK Integral Generation and Digestion System. *J. Comput. Chem.* 2023, *44* (3), 381-396.

[8] Zhao, Y., Truhlar, D. G., The M06 Suite of Density Functionals for Main Group Thermochemistry, Thermochemical Kinetics, Noncovalent interactions, Excited states, and Transition Elements: Two New Functionals and Systematic Testing of Four M06-class Functionals and 12 Other Functionals. *Theor. Chem. Acc.* 2008, *120* (1), 215-241.

[9] CYLview, 1.0b, Legault, C. Y., Université de Sherbrooke, 2009 (http://www.cylview.org).

[10] Y. X. Shi, W. H. Zhang, B. F. Abrahams, P. Braunstein and J. P. Lang, Fabrication of Photoactuators: Macroscopic Photomechanical Responses of Metal-Organic Frameworks to Irradiation by UV Light, *Angew. Chem. Int. Ed.*, **2019**, 58, 9453-9458.

[11] K. Yadava, G. Gallo, S. Bette, C. E. Mulijanto, D. P. Karothu, I. H. Park, R. Medishetty, P. Naumov, R. E. Dinnebier and J. J. Vittal, Extraordinary anisotropic thermal expansion in photosalient crystals, *IUCrJ*, **2020**, 7, 83-89.

[12] K. Yadava and J. J. Vittal, Photosalient Behavior of Photoreactive Zn(II) Complexes, *Cryst. Growth Des.*, **2019**, 19, 2542-2547.

[13] C. E. Mulijanto, H. S. Quah, G. K. Tan, B. Donnadieu and J. J. Vittal, Curved crystal morphology, photoreactivity and photosalient behaviour of mononuclear Zn(II) complexes, *IUCrJ*,

2017, 4, 65-71.

[14] R. Medishetty, S. C. Sahoo, C. E. Mulijanto, P. Naumov and J. J. Vittal, Photosalient Behavior of Photoreactive Crystals, *Chem. Mater.*, **2015**, 27, 1821-1829.